

An SIRS-model considering waning efficiency and periodic re-vaccination

Joseph Páez Chávez^{a,e}, Aytül Gökçe^b, Thomas Götz^c, Burcu Gürbüz^{d,f}

^aCenter for Applied Dynamical Systems and Computational Methods (CADSCOM), Faculty of Natural Sciences and Mathematics, Escuela Superior Politécnica del Litoral, P.O. Box 09-01-5863, Guayaquil, Ecuador

^bOrdu University, Faculty of Science and Letters, Department of Mathematics, 52200 Ordu, Turkey

^cMathematical Institute, University of Koblenz, D-56070 Koblenz, Germany

^dInstitut für Mathematik, Johannes Gutenberg-Universität Mainz, Staudingerweg 9, 55099 Mainz, Germany

^eCenter for Dynamics, Department of Mathematics, TU Dresden, D-01062 Dresden, Germany

^fInstitute for Quantitative and Computational Biosciences (IQCB), Johannes Gutenberg University Mainz, 55128 Mainz, Germany

Abstract

In this paper, we extend the classical SIRS (Susceptible-Infectious-Recovered-Susceptible) model from mathematical epidemiology by incorporating a vaccinated compartment, V, accounting for an imperfect vaccine with waning efficacy over time. The SIRS_V-model divides the population into four compartments and introduces periodic re-vaccination for waning immunity. The efficiency of the vaccine is assumed to decay with the time passed since the vaccination. Periodic re-vaccinations are applied to the population. We develop a partial differential equation (PDE) model for the continuous vaccination time and a coupled ordinary differential equation (ODE) system when discretizing the vaccination period. We analyze the equilibria of the ODE model and investigate the linear stability of the disease-free equilibrium (DFE). Furthermore, we explore an optimization framework where vaccination rate, re-vaccination time, and non-pharmaceutical interventions (NPIs) are control variables to minimize infection levels. The optimization objective is defined using different norm-based measures of infected individuals. A numerical analysis of the model's dynamic behavior under varying control parameters is conducted using path-following methods. The analysis focuses on the impacts of vaccination strategies and contact limitation measures. Bifurcation analysis reveals complex behaviors, including bistability, fold bifurcations, forward and backward bifurcations, highlighting the need for combined vaccination and contact control strategies to manage disease spread effectively.

Keywords: Epidemiological modeling, Stability, Bifurcation analysis, Optimal control, Numerical continuation

1. Introduction

Mathematical models have been essential to understanding the spread and control of infectious diseases, with the classical SIR (Susceptible-Infectious-Recovered) model being one of the most widely used frameworks in epidemiology. This model has been fundamental in analyzing the transmission dynamics of many infectious diseases by partitioning the population into susceptible, infected, and recovered individuals [1]. However, several complexities of the real world, such as waning immunity and vaccine dynamics, require extensions to the standard SIR-model to capture the full range of disease transmission and control efforts. Specifically, accounting for waning vaccine efficiency and periodic re-vaccination is critical to designing effective immunization strategies, especially for diseases where immunity is not permanent [2], [3]. For diseases such as pertussis, influenza, and COVID-19, waning immunity following natural infection or vaccination has been previously studied [4]. Such waning immunity can lead to a growing pool of susceptible individuals over time, increasing the likelihood of subsequent outbreaks. To address this, many public health strategies include periodic re-vaccination, especially for vaccines that do not provide lifelong immunity. Incorporating these factors into an SIR-based framework provides a more realistic representation of disease dynamics, especially in populations undergoing periodic vaccination campaigns [5], [6].

On the other hand, SIR-based models are used to develop new mathematical models for complex systems. In recent years, the SIR-model has been extended in various ways to address the complexity of infectious diseases with vaccination and waning immunity. Ehrhardt et al. (2019) present a comprehensive SIR-based model that accounts for both vaccination and waning immunity, highlighting the importance of incorporating these factors for a realistic representation of disease dynamics [7]. Sun and Yang further explore global outcomes in an SIRS-model, examining the effects of vaccination and isolation on disease control and demonstrating that isolation can significantly reduce infection rates [8]. González and Villena (2010) analyze the spatial dynamics of vaccination using a spatial SIRS-V model, emphasizing how spatial factors influence the spread of infectious diseases and vaccination strategies [9]. In addition, Elbasha et al. (2011) explore the dynamics of an SIRS-model that incorporates natural and vaccine-induced immunity, highlighting the implications of waning immunity for disease re-emergence and vaccination efforts [10]. Barbarossa and Röst (2015) examined immune status-structured populations, providing a detailed immuno-epidemiological perspective on how waning immunity and immune boosting can shape epidemic dynamics, highlighting the importance of immune memory and boosting events in disease management [11]. Together, these studies highlight the necessity of incorporating vaccination, waning immunity, and spatial considerations into epidemiological models to improve disease management strategies [12].

In this paper, we study a modified model as an extension of the classical SIRS-model that incorporates both waning vaccine efficacy and periodic re-vaccination, which are critical for managing diseases with incomplete or time-limited immunity. We introduce a the vaccination age x as the time elapsed since the (last) vaccination of an individual. The vaccinated compartment itself then depends both on time and vaccination age. The declining efficacy of the vaccine is modeled by a decreasing function that reflects the gradual reduction in immune protection conferred by vaccination [13]. Individuals in the vaccinated compartment are periodically re-vaccinated, which helps to maintain immunity in the population. The present extension enables to analyze both the direct effects of vaccination as well as the relationship between vaccination schedules, waning immunity, and the subsequent impact on the transmission dynamics of disease.

The remainder of this paper is organized as follows. In Section 2, the mathematical formulation of the SIRS-V-model with continuous vaccination age is presented. We briefly discuss the equilibria of this PDE model showing a parameter window where two endemic equilibria may co-exist. In Section 3 we discretize the vaccination age to reduce the model to a coupled, but high-dimensional ODE system. Again, we can discuss its equilibria that agree with the ones of the PDE model. The linear stability of the disease-free equilibrium is analyzed, and the basic reproduction number of the model is computed. In Section 4, we introduce the numerical continuation techniques used to explore the parameter space and investigate the impact of NPIs and we present numerical simulations of various disease control strategies, highlighting the effectiveness of combined vaccination and contact restriction policies. Finally, Section 5 is devoted to a discussion of the implications of the findings and the future directions of research.

2. SIRS-V-PDE-model with continuous vaccination age

We consider a classical SIRS-model from mathematical epidemiology and extend it introducing a vaccinated compartment. The entire population N is subdivided into the susceptible compartment S , the infected compartment I , the recovered compartment R and the vaccinated compartment V . Susceptible individuals get infected with rate β when in contact with an infected. Infected individuals recover with rate γ and recovered individuals lose their immunity with rate α and become susceptible again. For the vaccinated individuals, we introduce the time x elapsed since vaccination, called the *vaccination age*. The vaccine is assumed to be *imperfect* and its waning efficiency is modeled by a decreasing function $\omega(x)$ depending on the vaccination age x . The probability, that a vaccinated individual gets infected is given by $1 - \omega$. To partially compensate for the waning efficiency, we assume periodic update vaccinations, i.e. individuals that have been vaccinated P time units ago, receive a new vaccination.

Modeling the vaccination age x as a continuous variable, we arrive at a PDE model.

$$\frac{dS}{dt} = -\beta S \frac{I}{N} - \nu S + \alpha R, \quad (1a)$$

$$\frac{dI}{dt} = \beta \frac{I}{N} \left(S + \int_0^P (1 - \omega(x)) V(t, x) dx \right) - \gamma I, \quad (1b)$$

$$\frac{dR}{dt} = \gamma I - \alpha R, \quad (1c)$$

and a transport through time and vaccination age

$$\frac{\partial V}{\partial t} + \frac{\partial V}{\partial x} = -\beta \frac{I}{N} (1 - \omega(x)) V(t, x). \quad (1d)$$

The re-vaccination at time $x = P$ leads to the conditions

$$V(t, 0) = \nu S + V(t, P^-), \quad (1e)$$

$$V(t, P^+) = 0. \quad (1f)$$

Here $V(t, P^-) := \lim_{x \nearrow P^-} V(t, x)$ denotes the left-sided limit of $V(t, \cdot)$ at $x = P$ and $V(t, P^+)$ analogously denotes the right-sided limit.

If NPIs are applied to complement the vaccination campaign, we assume that these NPIs affect the transmission rate β , i.e.

$$\beta(t) := \beta_0 (1 - \rho(t)), \quad (2)$$

where $\rho \in [0, 1]$ denotes the severity of the restrictions, $\rho = 0$ means no restrictions and $\rho = 1$ means total lockdown.

To compute (temporal) equilibria of the PDE model, we assume $\omega(x) = \omega$ to be independent of the vaccination age x . The Eqns. (1c) and (1a) yield $R^* = \frac{\gamma}{\alpha} I^*$ and $S^* = \frac{\gamma N}{\beta I^* + \nu N} I^*$. The transport Eqn. (1d) reads in the temporal equilibrium as $\partial_x V^* = -\frac{\beta(1-\omega)}{N} I^* V^*$ and hence

$$V^*(x) = V_0^* \exp \left[-\frac{(1-\omega)\beta}{N} I^* x \right].$$

In the infection equation (1b), the integral runs effectively only over the interval $0 \leq x \leq P$, since at time P , individuals get re-vaccinated and hence there are no individuals with vaccination age larger than P . We obtain in the equilibrium either the trivial solution $I^* = 0$ or

$$\frac{\beta}{N} \left(\frac{\gamma N I^*}{\beta I^* + \nu N} + V_0^* (1 - \omega) \int_0^P \exp \left[-\frac{(1-\omega)\beta}{N} I^* x \right] dx \right) - \gamma = 0,$$

and after equating the integral and resorting terms, we arrive at

$$\frac{\beta \gamma I^*}{\beta I^* + \nu N} + \frac{V_0^*}{I^*} \left(1 - \exp \left[-\frac{\beta(1-\omega)P}{N} I^* \right] \right) - \gamma = 0,$$

and finally

$$V_0^* = \frac{\nu \gamma N}{\nu N + \beta I^*} \left(1 - \exp \left[-\frac{\beta(1-\omega)P}{N} I^* \right] \right)^{-1} I^*.$$

The equation for the total population $N = S^* + I^* + R^* + \int_0^P V^*(x) dx$ renders an equation for I^*

$$N = \frac{\gamma N}{\nu N + \beta I^*} I^* + \frac{\gamma}{\alpha} I^* + I^* + \frac{\nu \gamma N^2}{\beta(1-\omega)(\nu N + \beta I^*)}.$$

Introducing $z := I^*/N$, $1/R := \gamma/\beta$, $\lambda := \frac{\nu}{\beta}$ and $\delta := \frac{\gamma}{\alpha}$, we get

$$1 = \frac{z/R}{\lambda + z} + (1 + \delta)z + \frac{\lambda}{R(1-\omega)(\lambda + z)},$$

or

$$0 = z^2 + \left[\frac{1-R}{R(1+\delta)} + \lambda \right] z + \left[\frac{1}{R(1-\omega)} - 1 \right] \frac{\lambda}{1+\delta} =: f(z). \quad (3)$$

Therefore, we arrive at a quadratic equation for z , that needs to be solved for $0 < z \leq 1$ to obtain a meaningful endemic equilibrium. If $f(0) \cdot f(1) < 0$, then there exists exactly one endemic equilibrium $0 < z < 1$. For $f(1)$ we get

$$\begin{aligned} f(1) &= 1 + \frac{1-R}{R(1+\delta)} + \lambda + \left[\frac{1}{R(1-\omega)} - 1 \right] \frac{\lambda}{1+\delta}, \\ &= \frac{1}{1+\delta} \left[(1+\lambda)(1+\delta) - \frac{R-1}{R} - \lambda \left(1 - \frac{1}{R(1-\omega)} \right) \right], \\ &= \frac{1}{1+\delta} \left[\delta(1+\lambda) + \frac{1}{R} + \frac{\lambda}{R(1-\omega)} \right] > 0. \end{aligned}$$

Thus $f(1) > 0$ always and the only option to get exactly one endemic equilibrium is $f(0) < 0$ or $R > \frac{1}{1-\omega} \geq 1$.

In order to obtain two endemic equilibria, the following conditions should be satisfied:

1. $f(0) > 0$, i.e. $R < \frac{1}{1-\omega}$ or $\frac{1}{R} > 1-\omega$.
2. The minimum for f to be located at $0 < z_m < 1$. Then we have

$$z_m := -\frac{1}{2} \left[\frac{1-R}{R(1+\delta)} + \lambda \right],$$

and hence

$$1 - (2+\lambda)(1+\delta) < \frac{1}{R} < 1 - \lambda(1+\delta).$$

The above two conditions together imply $\omega > \lambda(1+\delta)$ for the possibility to have two endemic equilibria.

3. $f(z_m) < 0$. We have

$$f(z_m) = \left[\frac{1}{R(1-\omega)} - 1 \right] \frac{\lambda}{1+\delta} - \frac{1}{4} \left[\frac{1-R}{R(1+\delta)} + \lambda \right]^2.$$

Here the condition $f(z_m) < 0$ reads as

$$4 \frac{\lambda(1+\delta)}{1-\omega} \left(\frac{1}{R} - (1-\omega) \right) < \left(\frac{1}{R} - (1-\lambda(1+\delta)) \right)^2.$$

So, if $\omega > \lambda(1+\delta)$, there is some region for R , where two endemic equilibria could be possible. In terms of $\frac{1}{R}$, the lower bound of this region is given by $\max(1-\omega, 1-(2+\lambda)(1+\delta))$ and the upper bound equals

to the intercept of the linear function $4\frac{\lambda(1+\delta)}{1-\omega} \left(\frac{1}{R} - (1-\omega)\right)$ and the parabola $\left(\frac{1}{R} - (1-\lambda(1+\delta))\right)^2$.

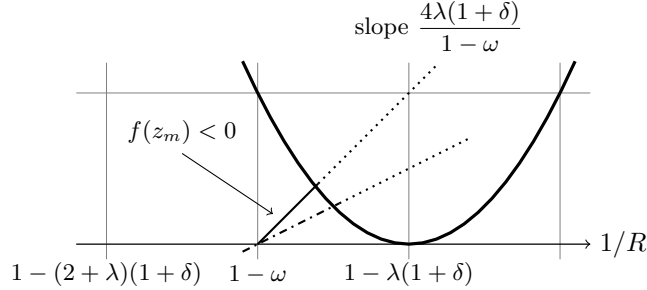


Figure 1: Graphical sketch of the condition $f(z_m) < 0$ for the existence of two equilibria.

3. SIRS_V-ODE-model with discrete vaccination age

Modeling the vaccination age x as a discrete variable, we arrive at a coupled ODE system. Let $k = 0, \dots, P$ denote the discrete vaccination ages equal to the time steps (days) elapsed since vaccination and let V_k denote the number of individuals of vaccination age k . Re-vaccination is applied to all individuals of P time units, i.e. individual of vaccination age $P - 1$ get re-vaccinated at the next time step and have vaccination age 0 afterwards. The waning effect of the vaccination is described by a decreasing sequence ω_k . Then the SIRS_V-model can now be written as

$$S' = -\beta S \frac{I}{N} - \nu S + \alpha R, \quad (4a)$$

$$I' = \beta \frac{I}{N} \left(S + \sum_{k=0}^{P-1} (1 - \omega_k) V_k \right) - \gamma I, \quad (4b)$$

$$R' = \gamma I - \alpha R, \quad (4c)$$

$$V_0' = \left(1 - \beta(1 - \omega_{P-1}) \frac{I}{N} \right) V_{P-1} - V_0 + \nu S, \quad (4d)$$

$$V_k' = \left(1 - \beta(1 - \omega_{k-1}) \frac{I}{N} \right) V_{k-1} - V_k \quad \text{for } k = 1, \dots, P - 1. \quad (4e)$$

For later reference, we introduce the state vector $Z = (S, I, R, V_0, \dots, V_{P-1}) \in \mathbb{R}^{P+3}$ of the above ODE system written shortly as $Z' = \Phi(Z)$. In this setting the total population $N = \sum_{j=1}^{P+3} Z_j = S + I + R + \sum_{k=0}^{P-1} V_k$ remains constant.

Again, NPIs can be included in the transmission rate β , see Eqn. (2)

The disease free equilibrium (DFE) Z^0 of the ODE-model equals to $I^0 = 0$ and hence $R^0 = 0$. The remaining compartments differ depending on the vaccination rate ν . In case of no vaccinations, i.e. $\nu = 0$, we get no vaccinated individuals at all, i.e. $V_k^0 = 0$ for all $k = 0, \dots, P$ and all individuals remain susceptible, $S = N$. In the other case $\nu > 0$, the susceptible and not vaccinated compartment gets empty, i.e. $S^0 = 0$ and due to Eqns. (4d),(4e), the vaccinated distribute evenly over all compartments, i.e. $V_k^0 = \frac{N}{P}$ for all $k = 0, \dots, P - 1$.

To compute the basic reproduction number of our model system, we use the next-generation matrix approach by van den Driessche and Watmough [14]. The ODE system (4) has only one infectious compartment I and hence

$$\mathcal{R}_0 = \frac{\beta}{\gamma N} \left(S^0 + \sum_{k=0}^{P-1} (1 - \omega_k) V_k^0 \right).$$

In case of $\nu = 0$, i.e. $S^0 = N$ and $V_k^0 = 0$ for all k , this simplifies to the well-known basic reproduction number of the standard SIR-model

$$\mathcal{R}_{0,\nu=0} = \frac{\beta}{\gamma}.$$

In the other case $\nu > 0$, we have $S^0 = 0$ and $V_k^0 = \frac{N}{P}$. Hence

$$\mathcal{R}_{0,\nu>0} = \frac{\beta}{P\gamma} \sum_{k=0}^{P-1} (1 - \omega_k).$$

In case of constant $\omega_k \equiv \omega$, this simplifies to

$$\mathcal{R}_{0,\nu>0} = \frac{\beta}{\gamma}(1 - \omega).$$

If $\omega = 1$, i.e. a perfect vaccine, $\mathcal{R}_0 = 0$ and for $\omega = 0$, i.e. an effectless vaccine, we get $\mathcal{R}_0 = \frac{\beta}{\gamma}$; the basic reproduction number of the classical SIR-model.

To analyze endemic equilibria Z^* with $I^* > 0$, we again assume $\omega_k = \omega$ for all k for simplicity. We proceed similar to the PDE case; solving the ODE for R yields

$$R^* = \frac{\gamma}{\alpha} I^*.$$

Solving the recursion for V_k yields

$$V_k^* = c^k V_0^*,$$

where $c := 1 - \frac{\beta(1-\omega)}{N} I^*$. Note, that this recursion is only meaningful, i.e. non-oscillating and bounded, if $0 < c < 1$. Hence $z = \frac{I^*}{N} < \frac{1}{(1-\omega)\beta}$.

Solving the ODE for $V_0' = 0$ allows the computation of S^* :

$$S^* = \frac{1}{\nu} V_0^* (1 - c^P).$$

The equation for $I' = 0$ yields either the disease free equilibrium $I^0 = 0$ or the following equation

$$\frac{1}{\nu} V_0^* (1 - c^P) + (1 - \omega) V_0^* \sum_{k=0}^{P-1} c^k = \frac{\gamma}{\beta} N,$$

i.e.

$$V_0^* (1 - c^P) \left(\frac{1}{\nu} + \frac{1 - \omega}{1 - c} \right) = \frac{\gamma}{\beta} N.$$

And finally, the condition $N = S^* + I^* + R^* + \sum_{k=0}^{P-1} V_k^*$ yields

$$N = \frac{V_0^*}{\nu} (1 - c^P) + \frac{\alpha + \gamma}{\alpha} I^* + V_0^* \sum_{k=0}^{P-1} c^k = V_0^* (1 - c^P) \left(\frac{1}{\nu} + \frac{1}{1 - c} \right) + \frac{\alpha + \gamma}{\alpha} I^*.$$

Inserting $V_0^*(1 - c^P) = \frac{\gamma}{\beta}N \left(\frac{1}{\nu} + \frac{1-\omega}{1-c} \right)^{-1}$ yields

$$N = \frac{\gamma}{\beta}N \left(\frac{1}{\nu} + \frac{1-\omega}{1-c} \right)^{-1} \left(\frac{1}{\nu} + \frac{1}{1-c} \right) + \frac{\alpha + \gamma}{\alpha}I^*.$$

Setting $z = I^*/N$ we get

$$1 = \frac{\gamma}{\beta} \frac{\nu + \beta(1-\omega)z}{(1-\omega)(\beta z + \nu)} + \frac{\alpha + \gamma}{\alpha}z.$$

or using the same scaled constants $R = \frac{\beta}{\gamma}$, $\lambda = \frac{\nu}{\beta}$ and $\delta = \frac{\gamma}{\alpha}$ as in the PDE case

$$1 = \frac{\lambda + (1-\omega)z}{R(1-\omega)(\lambda + z)} + (1 + \delta)z.$$

Again, the same quadratic equation as (3) in the PDE case for z is to be solved.

To analyze the linear stability of the DFE $Z^0 = (0, 0, 0, \frac{N}{P}, \dots, \frac{N}{P})$ we introduce the Jacobian $\mathcal{J} = (J_{ij}) = \frac{\partial \Phi_i}{\partial Z_j} \Big|_{Z^0}$ of the ODE system (4) at the DFE Z^0 . Then

$$\mathcal{J} = \begin{pmatrix} -\nu & 0 & \alpha & 0 & 0 & 0 & \cdots & 0 \\ 0 & J_{II} & 0 & 0 & 0 & 0 & \cdots & 0 \\ 0 & \gamma & -\alpha & 0 & 0 & 0 & \cdots & 0 \\ \nu & J_{0I} & 0 & -1 & 0 & 0 & \cdots & 1 \\ 0 & J_{1I} & 0 & 1 & -1 & 0 & \cdots & 0 \\ 0 & J_{2I} & 0 & 0 & 1 & -1 & & 0 \\ \vdots & & \vdots & & \ddots & \ddots & \ddots & \vdots \\ 0 & J_{(P-1)I} & 0 & 0 & \cdots & 0 & 1 & -1 \end{pmatrix}, \quad (5)$$

where $J_{II} = \frac{\beta}{N} \sum_{k=0}^{P-1} (1 - \omega_k) V_k^* - \gamma = \frac{\beta}{P} \sum_{k=0}^{P-1} (1 - \omega_k) - \gamma$ and $J_{kI} = -\frac{\beta}{N} (1 - \omega_k) V_k^* = -\frac{\beta}{P} (1 - \omega_k)$.

The characteristic polynomial of \mathcal{J} equals

$$\det(\mathcal{J} - \lambda E) = (J_{II} - \lambda) \cdot (-\alpha - \lambda) \cdot (-\nu - \lambda) \cdot \det(\mathcal{C}_P - \lambda E),$$

where \mathcal{C}_P denotes the cyclic matrix

$$\mathcal{C}_P = \begin{pmatrix} -1 & 0 & 0 & \cdots & 1 \\ 1 & -1 & 0 & \cdots & 0 \\ 0 & 1 & -1 & \ddots & 0 \\ \vdots & \ddots & \ddots & \ddots & \vdots \\ 0 & \cdots & 0 & 1 & -1 \end{pmatrix} \in \mathbb{R}^{P \times P}.$$

Using Laplace with respect to the first row yields

$$\det(\mathcal{C}_P - \lambda E) = (-1 - \lambda)^P + (-1)^{P+1} = (-1)^P \left((1 + \lambda)^P - 1 \right).$$

Hence

$$\det(\mathcal{J} - \lambda E) = (-1)^P \cdot (J_{II} - \lambda) \cdot (\lambda + \alpha) \cdot (\lambda + \nu) \cdot \left((1 + \lambda)^P - 1 \right). \quad (6)$$

The last factor has the trivial root $\lambda = 0$ and all other roots are in the negative half plane $\text{Re}(\lambda) < 0$. If $J_{II} < 0$, then \mathcal{J} has a zero eigenvalue and all other eigenvalues in the negative half plane. The appearance

of a zero eigenvalue is obvious due to the conservation of the total population. The condition $J_{II} < 0$ is equivalent to $\mathcal{R}_{0,\nu>0} < 1$. Therefore the DFE Z^0 is linearly stable, if the basic reproduction number $\mathcal{R}_{0,\nu>0} < 1$.

Table 1: Description of the parameters of the SIRS ν -system (4).

Parameter	Value	Remark
N	1000	Total population
$S(0)$	995	Initial susceptibles
$I(0)$	5	Initial infected
$R(0)$	0	Initial recovered
$V_k(0)$	0	No vaccinated at the beginning
γ	0.1	Recovery period of 10 days
β	0.23	Infection rate
α	0.005	Loss of immunity after 200 days
ν	0.01	Vaccination rate
P	90	Vaccination update after 3 months
ω_k	$e^{-k/W}$	Waning efficiency of the vaccine, $W = 60$

In the sequel we will work with the ODE formulation of the SIRS ν -model.

4. Numerical study of the epidemiological SIRS ν -model

This section is devoted to a comprehensive numerical investigation of the dynamical behavior of the SIRS ν -ODE-model (4) when selected control parameters are varied. To this end, we will use path-following (continuation) methods implemented by the continuation software COCO [15]. Based on the MATLAB environment, this platform is focused on the numerical solution of continuation problems covering a wide range of analysis and detection capabilities available in classical continuations packages, such as AUTO [16] and MATCONT [17]. In this work two such COCO functionalities will be employed, namely, continuation and bifurcation detection of equilibria of parameter-dependent smooth odes, and that of multi-segment periodic solutions of piecewise-smooth systems, as will be explained in detail later.

4.1. Investigation of parameter-dependent equilibria of the model

For the numerical study of the epidemiological SIRS ν -model (4), it is important to note first that some parameters and variables presented in Table 1 span different orders of magnitude. This variation often impacts the precision and reliability of the results because of the set tolerances for determining convergence and estimating errors in COCO. This imbalance can make the computations less responsive to certain variations while being excessively sensitive to others. Hence, we re-scale the SIRS ν model (4) as shown below

$$S \leftarrow \frac{S}{N}, \quad I \leftarrow \frac{I}{N}, \quad V_k \leftarrow \frac{V_k}{N}, \quad k = 0, 1, \dots, P-1.$$

Moreover, since the overall population N remains constant, we will reduce the dimension of the system via the equation $R = N - S - I - \sum_{k=0}^{P-1} V_k$. Furthermore, although the numerical computations will be implemented using the re-scaling introduced above, the outcome will be presented in the original scale for better interpretation of the results.

To start our study, we will set the parameter values of the epidemiological SIRS ν -model (4) according to Table 1, but considering $\omega_k = 0.5$ constant, that is, we will assume a perfect vaccine with a fixed efficiency (no waning effect). Under this consideration, the dynamical response of system (4) obtained via direct numerical integration is presented in Fig. 2. This diagram displays the transient response for the following compartments of the model: S , I and V_k ($k = 0, 45, 89$). As can be observed in the diagram, with the chosen parameter values, the system exhibits a damped oscillatory behavior that eventually stabilizes over time into an endemic equilibrium, that is, a steady state where the disease persists within

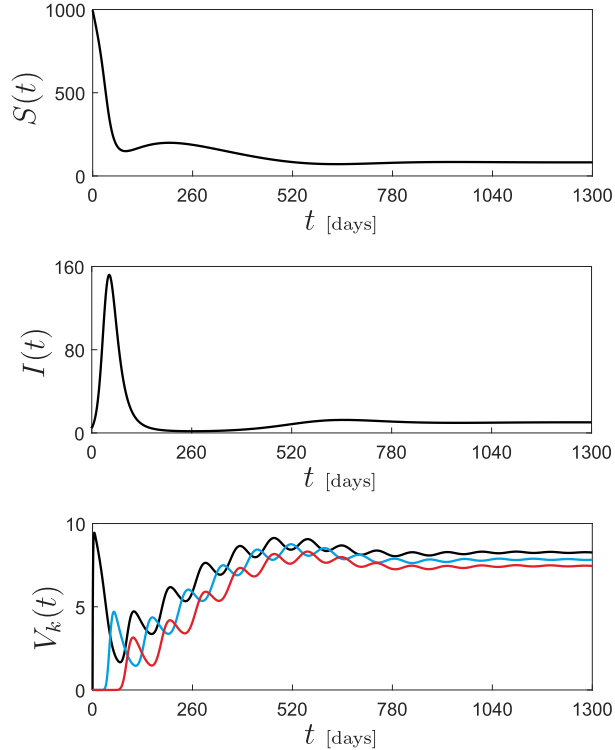


Figure 2: Simulation of the epidemiological SIRS model (4), calculated using the parameter values and initial conditions provided in Table 1, with $\omega_k = 0.5$ constant (no waning effect). The last graph shows time series of V_k -compartments for $k = 0$ (black), $k = 45$ (blue) and $k = 89$ (red).

the system. A notable feature of this dynamical response is the pulse-like outbreak of the disease observed during the first 100 days, reaching a peak of around 152 infections. After this, the infections consistently decrease owing to the effectiveness of the vaccination campaigns, although at the end such pharmaceutical intervention is not able to eradicate completely the disease. Furthermore, the V_k -compartments show a biologically consistent behavior, in that they activate themselves in the expected sequence, according to the proposed re-vaccination scheme.

Next, we will use numerical continuation methods to explore how variations in certain parameters affect the equilibrium and validate some of the analytical results derived in earlier sections. Specifically, our analysis will discuss the response of the endemic equilibrium to continuous variations of the infection rate β and vaccination rate ν . The results from the path-following analysis are presented in Fig. 3, panels (a)-(c). In these figures, the left vertical axis (in blue) shows the simulated infected compartment with respect to variations of the model parameters β or ν . The second vertical axis (right hand side, in red) displays the according reproduction number \mathcal{R}_0 .

Fig.3(a) shows the equilibria as the infection rate β changes. The diagram reveals that the reproduction number \mathcal{R}_0 is below 1, resulting in a stable disease-free equilibrium, as long as the infection rate is below the branching point BP1 at $\beta_0.2$. This is represented by the solid horizontal branch in the figure. As β increases, \mathcal{R}_0 also rises, crossing 1 from below at the branching point BP1.

At this point, the endemic equilibrium emerges and the disease-free equilibrium gets unstable through a forward bifurcation. For larger values of the infection rate, the disease persists and the number of infections grows as the infection rate increases. A different scenario arises when the vaccination rate ν is adjusted, as shown in Fig.3(b). As can be observed in the picture, for ν between 0 and 0.01 a strong reduction of the infections is achieved, thus showing the effectiveness of the proposed vaccination campaign. However, a more intensive (and expensive) vaccination policy produces no significant additional reduction, as can be verified during the numerical continuation of equilibria. From a mathematical perspective, this can be explained observing the response of the basic reproduction number \mathcal{R}_0 , which does

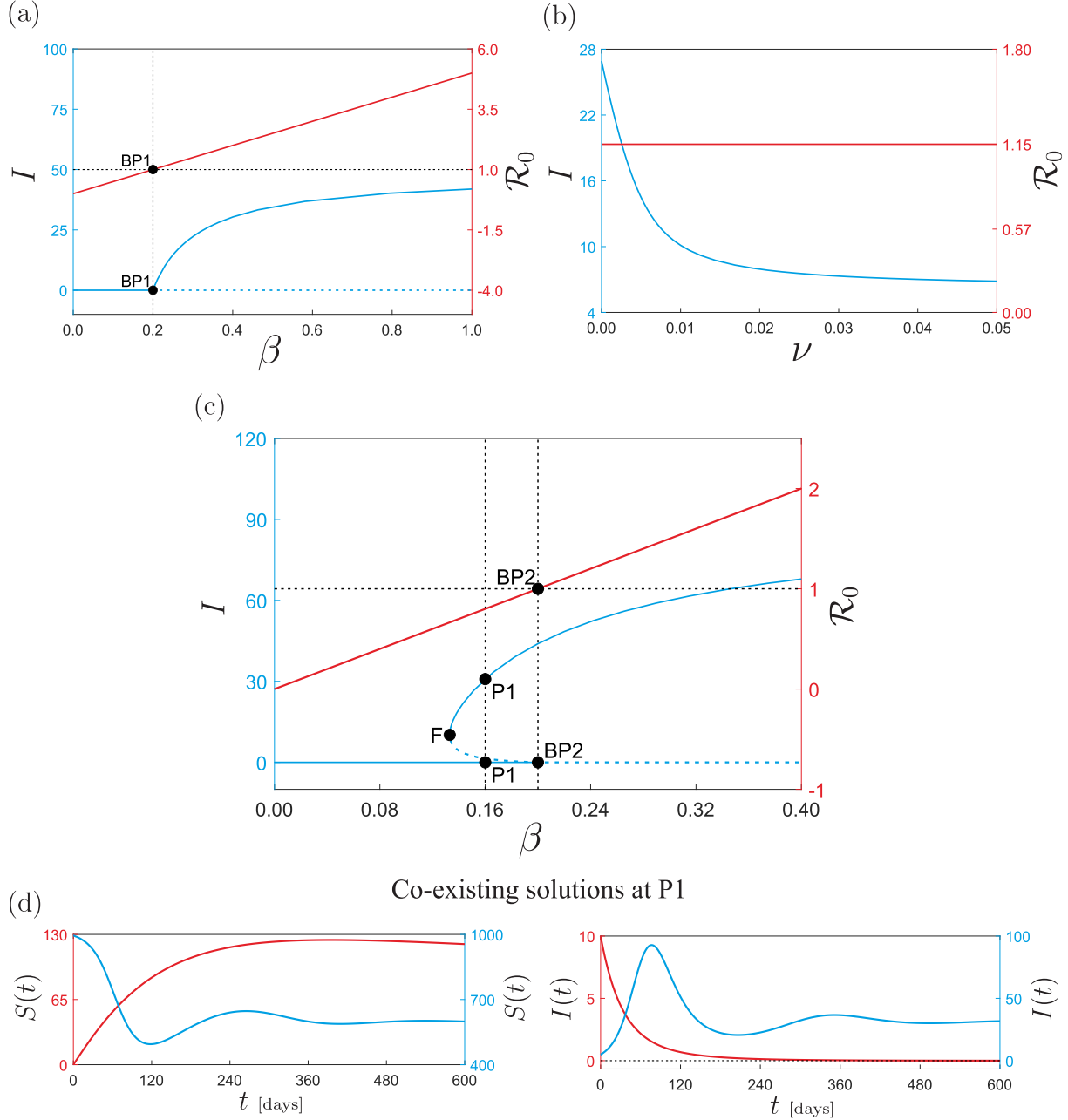


Figure 3: Numerical continuation of equilibrium points of system (4) with respect to β and ν . Panels (a) and (b) are calculated for the parameter set given in Fig. 2, while panel (c) is obtained for the same parameters, except for $\nu = 0.0003$ and $\alpha = 0.01$. Panels (a)–(c) display the infection compartment behavior at equilibrium on the left vertical axis (blue), the second vertical axes (right, in red) represent the basic reproduction number \mathcal{R}_0 . In these plots, solid blue lines indicate stable equilibrium branches, and dashed blue lines represent unstable equilibrium branches. Throughout the calculations, various critical points are identified, including the branching points BP1 and BP2 at $\beta = 0.2$, and the fold bifurcation F at $\beta \approx 0.13303$. Panel (d) presents time series for the system (4) at the test point P1 ($\beta = 0.16$), where two stable solutions co-exist.

not depend on ν (see red curve in Fig. 3(b)). This is due to the fact that for the disease-free equilibrium the susceptible compartment gets empty, and hence there is no new individuals to vaccinate at rate ν , as explained in the previous section. This means that vaccination alone cannot eliminate the disease, or even reduce the level of infected humans below an arbitrarily chosen level, if required.

In the previous section, our analytical study of the proposed epidemiological SIRS ν -model revealed the possibility of having a single endemic equilibrium (as the scenario discussed above) or two coexisting endemic equilibria. In order to verify this prediction, we will choose suitable parameter values according to the analytical calculations presented earlier in order to confirm numerically the expected behavior. The outcome is presented in Fig. 3(c), which was obtained for the same set of parameters as before, except for $\nu = 0.0003$ and $\alpha = 0.01$, chosen according to our analytical calculations. The continuation process detects of a backward bifurcation at BP2 ($\beta = 0.2$), which produces precisely the expected scenario, namely, the presence of coexisting endemic equilibria, one stable and one unstable. At high infection rates, the system exhibits a branch of endemic equilibria, shown in blue in the figure. This branch becomes unstable at a fold bifurcation F, occurring at approximately $\beta = 0.13303$. This fold bifurcation occurs, when a second endemic equilibrium appears, i.e. when the quadratic equation (3) allows for two real solutions corresponding to these two possible equilibria. Setting the discriminant of the quadratic equation (3) equal to zero yields

$$\beta_{\text{fold}} = \gamma - \nu(1 + \delta) \pm 2\sqrt{\gamma\nu(1 + \delta)}.$$

For the parameters chosen in Fig. 3(c), the larger of the two solution is given by $\beta \approx 0.133$, the fold bifurcation F. At this point, the endemic equilibrium branch shifts in the direction of increasing parameters and ends at the backward bifurcation BP2. Here, the basic reproduction number \mathcal{R}_0 crosses transversally the critical value 1 from below when the parameter increases over BP2.

It is important to note in the previous discussion that having $\mathcal{R}_0 < 1$ does not necessarily guarantee the disease to be eradicated. Between F and BP2, we find a bistable region, and the initial condition determines, whether, the system either approaches the disease-free or the endemic equilibrium. This is illustrated in Fig. 3(d) using the parameter value $\beta = 0.16$, which lies within the bistability range. From a practical standpoint, this presents a critical scenario where, even with $\mathcal{R}_0 < 1$, the sudden introduction of sufficient virus carriers into the population could drive the system toward an endemic equilibrium with high infection levels. Furthermore, once the system enters the endemic branch, reducing the infection rate β to bring \mathcal{R}_0 below 1 (as seen at BP2) is not enough to eradicate the disease. The infection rate must be reduced below the fold bifurcation F, at which point the disease-free equilibrium becomes globally stable.

4.2. Disease control considering contact restrictions

As the SARS-CoV-2 (COVID-19) pandemic in 2019 showed, one effective way to contain the disease is to impose contact restrictions (lockdowns) on the population, in combination to massive vaccination campaigns. In the previous section, our numerical study established that for the proposed epidemiological SIRS ν -model (4) vaccination alone is not enough to achieve an effective control of the number of infections, and therefore additional control strategies should be employed. Similar to the COVID-19 case, we will introduce contact restrictions in the model according to the functional response (2). Here, the function ρ is described by

$$\begin{cases} \rho(t) = 1, & I(t) = I_{\max}, \quad I'(t) > 0, \\ \rho'(t) = -\eta\rho(t), & \text{otherwise,} \end{cases} \quad (7)$$

with $0 \leq \rho(0) \leq 1$ and $t \geq 0$. From (2) one can see that the main role of the function ρ is to control the transmission rate β , where a full lockdown corresponds to $\rho = 1$ and no contact restrictions to $\rho = 0$. In model (7) it is assumed that full lockdown is applied when the number of infections reaches a predefined critical level I_{\max} . After this, the contact restrictions are relaxed gradually as the time progresses, assuming a simple exponential decay (which can of course follow any other decaying pattern, if required). The pace at which the restrictions are relaxed is controlled by the parameter $\eta > 0$. A small value (say close to 0) indicates that the restriction policies are strict, while η high means that the lockdowns do not last for too long. A numerical simulation of this control scheme is presented in Fig. 4

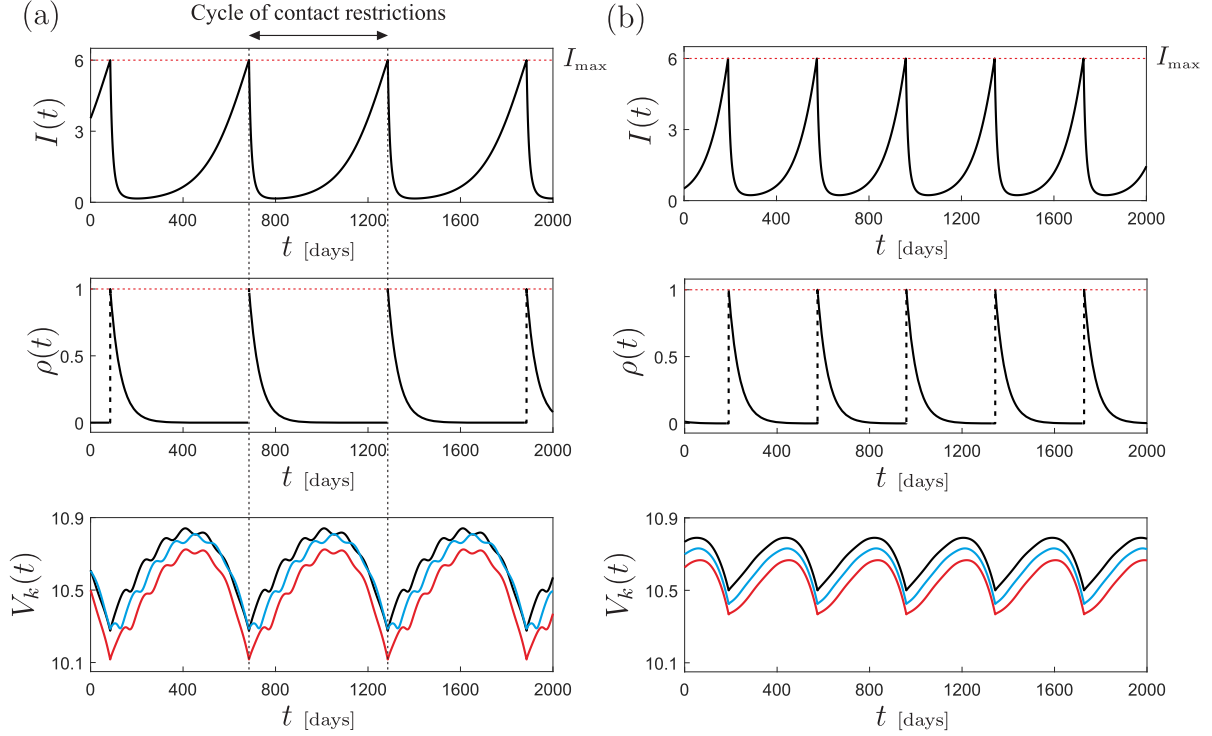


Figure 4: Simulation of the epidemiological SIRS model (4) subject to the contact restrictions (2) and (7), calculated for the parameter set provided in Table 1 with $\eta = \frac{1}{45}$ and $I_{\max} = 6$. The V_k -compartments follow the same color code as in Fig. 2. Panel (a) is calculated considering the waning effect, while panel (b) is computed for $\omega_k = 0.5$ constant (no waning).

showing two cases: with waning vaccine efficiency (ω_k variable, panel (a)) and fixed vaccine efficiency (ω_k constant, panel (b)).

4.3. Monitor and cost functions

Notice that according to the control scheme proposed in the previous section the peak of infections are restricted via the parameter I_{\max} . Every time the infection compartment reaches this value from below full lockdowns are activated, due to which the number of infections decreases, as can be observed in the simulation shown in Fig. 4. Therefore, one monitor function that we will consider in our investigation is the following

$$I_{\text{AVG}} = \frac{1}{T_0} \int_0^{T_0} I(t) dt, \quad (8)$$

where a bounded periodic response with period T_0 is assumed. This gives the average number of infections per period, which is a quantity that is independent from the peak infections I_{\max} . That is, for a fixed I_{\max} one may observe different levels of I_{AVG} when other parameters are adjusted, as will be seen later.

Another factor that will be examined in our study is the cost associated with the proposed control scheme. Specifically, we will consider two costs as follows

$$P_{\text{COST}} = \frac{1}{T_0} \int_0^{T_0} \frac{\rho(t)}{I(t)} dt \quad (\text{political cost}), \quad V_{\text{COST}} = \frac{\nu}{T_0} \int_0^{T_0} S(t) dt \quad (\text{vaccination cost}). \quad (9)$$

The first term can be interpreted as a measure of the political cost produced by the lockdown policies. When $\rho(t)$ decreases slowly and remains close to 1 (see previous section) it means that the contact restrictions are strict, and therefore the political cost should increase. If, however, such policy is applied

during a disease outbreak (i.e. high $I(t)$) then the lockdowns can be well justified among the population and hence the political cost reduces. On the contrary, if strict lockdowns are applied ($\rho(t)$ close to 1) during low level of infections ($I(t)$ close to 0), then the political cost grows, because such policy would seem completely unnecessary. On the other hand, the second term in (9) represents the cost of vaccination campaigns. It is taken to be the product of the average number of susceptible individuals during one period and the vaccination rate, which is an indicator of how many individuals are vaccinated in average and gives us insight as to how the associated costs behave.

4.4. Numerical study of the proposed disease control strategy

This section will present a numerical investigation of the dynamical behavior of the epidemiological SIRSV-model (4) considering contact restriction policies given by (2) and (7), with $\beta_0 = 0.23$ fixed. To this end, we will use the COCO-capabilities for numerical continuation of multi-segment periodic solutions for piece-smooth systems, since model (4) in combination with (2) and (7) falls within this category. For our investigation, we will consider the two cases displayed in Fig. 4: panel (a) including waning efficiency of the vaccine (decreasing ω_k) and panel (b) corresponding to $\omega_k = 0.5$ fixed (no waning).

Let us consider first the case of waning vaccine efficiency. The numerical continuation of the resulting periodic response with respect to the control parameter η is presented in Fig. 5(a). As explained earlier, this parameter determines how fast the contact restrictions are relaxed. Small values of this parameter indicate that the lockdowns are strict and only lifted slowly in time. This effect is reflected on the behavior of the average number of infections I_{AVG} , in an expected and consistent manner. In addition, Fig. 5(d) displays the behavior of the control costs defined in (9). As can be seen in this figure, the political cost and vaccination cost present decreasing and increasing behavior, respectively. The political cost reduces as the parameter η increases, since larger η means soft contact restrictions, which do not pose any discomfort to the population. The vaccination cost, however, increases due to the increasing number of average infections that after some time goes back to the susceptible population via the recovery compartment R (see (4)), and therefore the number of vaccinated individuals grows.

A different scenario is found when the vaccination rate ν is considered as control parameter. Fig. 5(b) shows the response of the average number of infections I_{AVG} as the parameter varies. Similar to the equilibrium case (see Fig. 3(b)) a strong reduction of average infections can be achieved over a short parameter window. Beyond that, the value of I_{AVG} stabilizes regardless of how strong the vaccination rate becomes. As for the control costs, one can see in Fig. 5(e) that again vaccination and political costs present different behaviors. As expected, the vaccination cost increases when ν grows. The political cost, on the contrary, increases significantly when the vaccination becomes smaller. This is due to the fact that as the vaccination campaigns weaken, the only remaining action to keep $I(t)$ below I_{max} is the contact restrictions through the function ρ , and, as discussed earlier, stronger restrictions increase the incurred political cost. This means that in order to keep the political costs under reasonable levels, both vaccination and lockdowns should be combined in a suitable manner.

Another feature observed during the numerical continuation of the periodic solutions with waning vaccine efficiency is the presence of an optimal level of vaccination rate. This is found for $\nu \approx 0.00227$ (point labeled Pmin), see Fig. 5(b). Here, a local minimum of average number of infections I_{AVG} is found, and one question that can be tackled here is whether the presence of this minimum is affected by the type of vaccine, namely, a perfect vaccine with constant efficiency (see solution in Fig. 4(b)) and a vaccine that loses effectiveness over time (waning effect). Therefore, we will also perform the numerical continuation of the system response shown in Fig. 4(b) (perfect vaccine) with respect to the vaccination rate ν , see Fig. 5(c). Here, it can be observed that there is no minimum anymore, which indicates that the type of vaccine plays an important role in choosing suitable vaccination rates, in terms of minimizing average number of infections, and not incurring in unnecessary increasing vaccination costs, see Figs. 5(b), (c), (e) and (f).

5. Conclusion

The SIRSV-model, described in this paper, provides a comprehensive framework for understanding the dynamics of infectious diseases in the presence of waning vaccine efficiency and periodic re-vaccination.

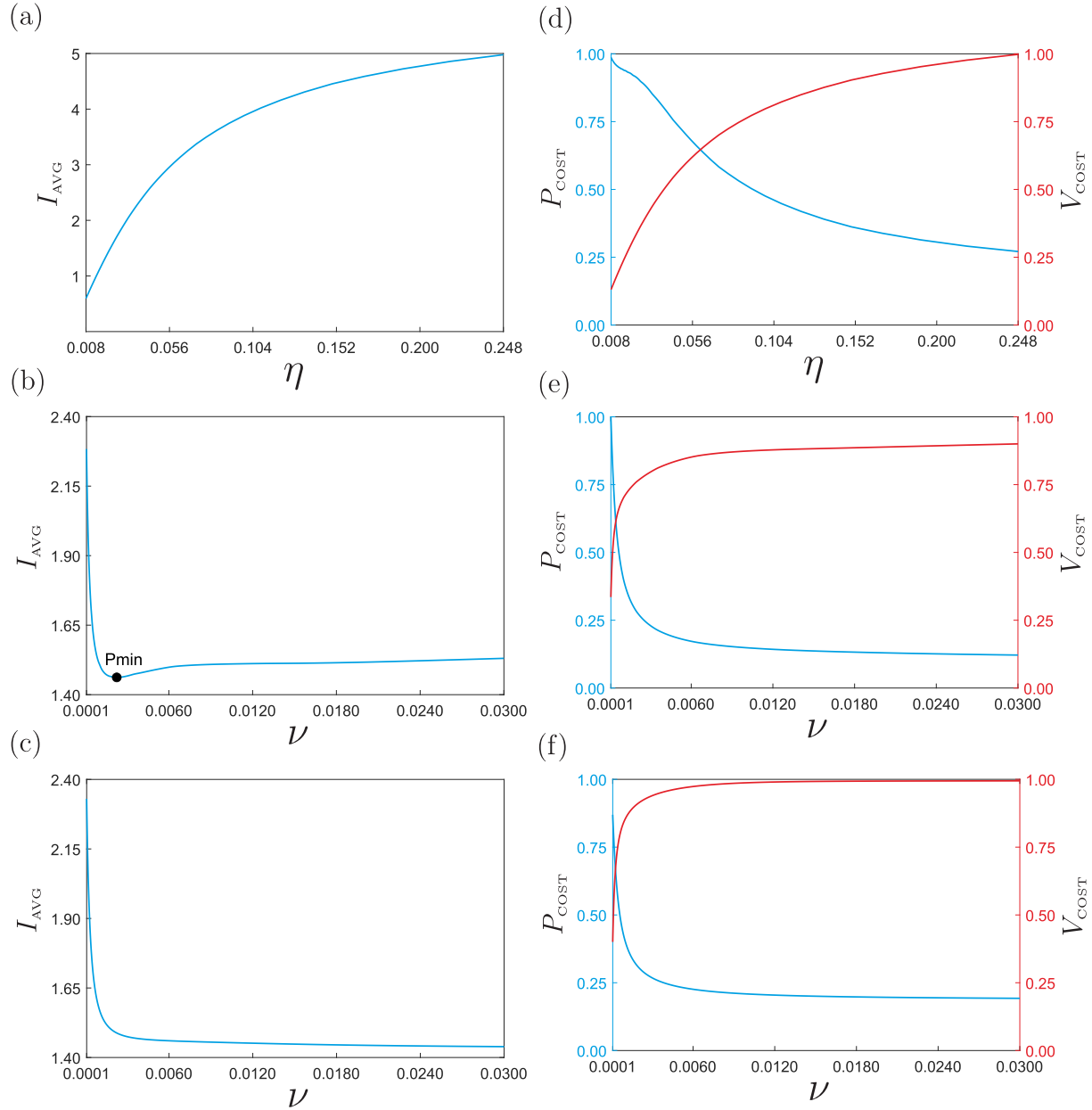


Figure 5: Numerical continuation of the periodic solution shown in Fig. 4 with respect to η and ν . Panels (a)–(c) show the behavior of the average infection occurrences per period. Panels (d)–(f) display the variation of the political cost (left vertical axis, blue) and vaccination cost (right vertical axis, red) as the control parameter changes. All calculations are performed using the periodic response in Fig. 4(a) (waning effect), except for the curves in panels (c) and (f), which correspond to the solution in Fig. 4(b) (no waning). In these diagrams, both political and vaccination costs are normalized between 0 and 1 for better comparison.

By incorporating both vaccination and re-vaccination processes, along with NPIs, the model is able to capture the critical elements required for effective disease control in real-world scenarios. Our analysis demonstrates that while vaccination plays a vital role in reducing the spread of infections, the waning efficiency of vaccines presents a significant challenge to long-term immunity. The periodic re-vaccination strategy, as modeled here, helps to mitigate this effect, but does not eliminate the risk of endemic disease. Through equilibrium and stability analysis, we identified the conditions under which the disease-free equilibrium is stable and the circumstances that lead to the persistence of endemic equilibria.

One of the principal findings from our numerical simulations is the importance of combining vaccination with timely NPIs, such as contact restrictions. Our results show that NPIs can significantly reduce the average number of infections, especially when vaccine efficiency wanes over time. However, the model also demonstrates a trade-off between the costs of NPIs, vaccination, and the effectiveness of disease control. The optimization of these control measures is of critical importance for the design of policies that minimize both the number of infections and the economic and political costs associated with interventions.

Future work can focus on refining the model by incorporating more realistic vaccination schedules, heterogeneous populations, and age-structured dynamics. Furthermore, the cost functions introduced in this paper can be further developed to include more detailed economic and social factors, thus providing a more comprehensive tool for public health decision-making [18], [19].

References

- [1] W. O. Kermack and A. G. McKendrick, “A contribution to the mathematical theory of epidemics,” *Proceedings of the Royal Society A: Mathematical, Physical and Engineering Sciences*, vol. 115, no. 772, pp. 700–721, Aug. 1927.
- [2] R. Anderson, *Infectious diseases of humans: dynamics and control*. New York: Cambridge University Press, 1991.
- [3] H. W. Hethcote, “The mathematics of infectious diseases,” *SIAM Review*, vol. 42, no. 4, pp. 599–653, 2000.
- [4] S. A. Plotkin, “Correlates of protection induced by vaccination,” *Clinical and Vaccine Immunology*, vol. 17, no. 7, pp. 1055–1065, 2010.
- [5] P. Doenges, T. Götz, N. Kruchinina, T. Krüger, K. Niedziewski, V. Priesemann, and M. Schäfer, “SIR model for households,” *SIAM Journal on Applied Mathematics*, vol. 84, no. 4, pp. 1460–1481, 2024.
- [6] A. Gökçe, B. Gürbüz, and A. D. Rendall, “Dynamics of a mathematical model of virus spreading incorporating the effect of a vaccine,” *Nonlinear Analysis: Real World Applications*, vol. 78, p. 104097, 2024.
- [7] M. Ehrhardt, J. Gašper, and S. Kilianová, “SIR-based mathematical modeling of infectious diseases with vaccination and waning immunity,” *Journal of Computational Science*, vol. 37, p. 101027, 2019.
- [8] C. Sun and W. Yang, “Global results for an SIRS model with vaccination and isolation,” *Nonlinear Analysis: Real World Applications*, vol. 11, pp. 4223–4237, 2010.
- [9] E. González and M. J. Villena, “On the spatial dynamics of vaccination: A spatial SIRS–V model,” *Computers & Mathematics with Applications*, vol. 80, pp. 733–743, 2020.
- [10] E. H. Elbasha, C. N. Podder, and A. B. Gumel, “Analyzing the dynamics of an SIRS vaccination model with waning natural and vaccine-induced immunity,” *Nonlinear Analysis: Real World Applications*, vol. 12, pp. 2692–2705, 2011.

- [11] M. V. Barbarossa and G. Röst, “Immuno-epidemiology of a population structured by immune status: a mathematical study of waning immunity and immune system boosting,” *Journal of Mathematical Biology*, vol. 71, pp. 1737–1770, 2015.
- [12] O. N. Bjørnstad, K. Shea, M. Krzywinski, and N. Altman, “The SEIRS model for infectious disease dynamics,” *Nature Methods*, vol. 17, no. 6, pp. 557–559, 2020.
- [13] H. J. Wearing and P. Rohani, “Estimating the duration of pertussis immunity using epidemiological signatures,” *PLoS Pathogens*, vol. 5, no. 10, p. e1000647, 2009.
- [14] P. Van den Driessche and J. Watmough, “Reproduction numbers and sub-threshold endemic equilibria for compartmental models of disease transmission,” *Mathematical Biosciences*, vol. 180, no. 1-2, pp. 29–48, 2002.
- [15] H. Dankowicz and F. Schilder, *Recipes for continuation*. Computational Science and Engineering, Philadelphia: SIAM, 2013.
- [16] E. J. Doedel, A. R. Champneys, T. F. Fairgrieve, Y. A. Kuznetsov, B. Sandstede, and X.-J. Wang, *Auto97: Continuation and bifurcation software for ordinary differential equations (with HomCont)*. Computer Science, Concordia University, Montreal, Canada, 1997. Available at <http://cmv1.cs.concordia.ca>.
- [17] A. Dhooge, W. Govaerts, and Y. A. Kuznetsov, “MATCONT: A MATLAB package for numerical bifurcation analysis of ODEs,” *ACM Trans. Math. Software*, vol. 29, no. 2, pp. 141–164, 2003.
- [18] S. Moore, E. M. Hill, M. J. Tildesley, L. Dyson, and M. J. Keeling, “Vaccination and non-pharmaceutical interventions for COVID-19: a mathematical modelling study,” *The Lancet Infectious Diseases*, vol. 21, no. 6, pp. 793–802, 2021.
- [19] K. P. Wijaya, J. Páez Chávez, and T. Götz, “A dengue epidemic model highlighting vertical-sexual transmission and impulsive control strategies,” *Applied Mathematical Modelling*, vol. 95, pp. 279–296, 2021.